Research Performance Progress Report

Project Title:	Low Cost Heliostat Development
Project Period:	08/01/10 – 12/31/13
Budget Period:	Phase 2; 12/11/12 – 12/31/13
Budget Period Budget:	$1,019,181
Reporting Period:	12/11/12 – 12/31/13
Reporting Frequency:	Quarterly
Submission Date:	04/31/13
Recipient:	HiTek Services, Inc.
Recipient DUNS #:	025139861
Address:	7234 Hwy. 431 South Owens Cross Roads, AL 35763
Award Number:	DE-EE0003593
Awarding Agency:	DOE EERE SETP CSP subprogram
Working Partners:	University of Alabama - Huntsville
Cost-Sharing Partners:	University of Alabama - Huntsville

Principal Investigator: Stephen Kusek
President
Phone: 256-539-0380
Fax: 256- 539 -0370
Email: kusek@hitek-services.com

GO Contracting Officer: Clay Pfrangle

Technology Project Officer: Thomas Rueckert

DOE Technical Manager: Mark Lausten

Project Objective:

The project objectives were:

1. To develop the means for determining the optimal size of a heliostat in terms of applied forces, moments, manufacturing learning curve effects, O&M, and optical efficiency.
2. Use those means to determine the appropriate heliostat size for a typical Az/El heliostat to minimize cost.
3. Develop and demonstrate the performance of a novel, low-cost heliostat

Introduction:

The heliostat field in a central receiver plant makes up roughly one half of the total plant cost. As such, cost reductions for the installed heliostat price greatly impact the overall plant cost and hence the plant's Levelized Cost of Energy. The general trend in heliostat size over the past decades has been to make them larger. One part of our thesis has been that larger and larger heliostats may drive the LCOE up instead of down due to the very nature of the precise aiming and wind-load requirements for typical heliostats. In other words, it requires more and more structure to precisely aim the sunlight at the receiver as one increases heliostat mirror area and that it becomes counter-productive, cost-wise, at some point.

There are many cost trade-offs. As an example, lower field wiring costs for larger heliostats versus lower specific structure costs for smaller heliostats. The "correct" size is not intuitively obvious and there may be different answers for different system requirements. A major component of this project was to develop a methodology to perform a rigorous analysis of optimal heliostat size for a nominal 100MWe base load solar plant with a capacity factor of 75% that uses a typical single-pedestal azimuth/elevation driven heliostat. The results of that work point toward an "optimal" size around $10m^2$. The second overarching task is to then develop and test a "low-cost" heliostat of that size and with some new features to further reduce its production cost. These features are: (1) a novel multi-stage azimuth chain drive that has the inherent ability to better absorb dynamic wind loads for long life, and (2) a control system that removes the need for heliostat field wiring dubbed the autonomous heliostat. We believe these features will help drive the heliostat field cost down while creating a heliostat that requires less field replacement due to repeated wind loading over the anticipated power plant lifetime.

Work Planned for this Quarter: The project has ended.

Project Approach:

The approach used to determine an "optimal" heliostat size was to define an analytical methodology wherein the hardware costs are separated by cost categories. In its simplest form, these categories are (1) constant cost per unit area, (2) members where the cost varies with imposed torque, and (3) constant per heliostat regardless of size. The costs from DOE published data was then used with this methodology to determine an optimal heliostat size based upon the many assumptions used in the analysis.

The innovative hardware (azimuth drive and autonomous controls) used in the heliostat development are derived from previous field and lab experience and are design perturbations that are intended to reduce cost. The new damping mechanism(s) for the azimuth drive will be developed using a modified existing chain drive to experimentally verify damping mechanism concepts.

Project Results and Discussion:

This project was originally proposed as a three phase project. After completion of Phase I, the project was modified into a two-phase project culminating in the fabrication and testing of a prototype heliostat. Phase I had two objectives: (1) to conduct analyses to find an optimal heliostat size and (2) to develop a novel low-cost heliostat. The Phase I work was divided into four primary tasks:

Task 1 – Heliostat Size Analysis,

Task 2 – Heliostat Reflector,

Task 3 – Drive Unit, and

Task 4 – Tracking Control System.

This phase of the project ended in April of 2012 and a Phase I report was submitted. The single most important accomplishment of Phase I was the development of a generic method to find an optimally sized heliostat. Using cost data from previously published DOE reports, this method showed that the cost-optimal heliostat was much smaller than many in the field had been developing. For the chosen set of inputs, it was shown that a heliostat size of around $10m^2$ was much closer to a cost minimum than a $148m^2$ heliostat.

Phase II of the project was divided into five major tasks:

Task 1 – Heliostat Size, Load, and Market Analysis,

Task 2 – Drive Unit,

Task 3 – Heliostat Control,

Task 4 – Heliostat Integration, and

Task 5 – Prototype Heliostat Testing.

This phase ended in December 2013; however, we were unable to complete all the proposed work by then and an additional schedule extension was not granted. The two most important accomplishments of this phase were the publications detailing the heliostat sizing work in Task 1 and the development of the autonomous heliostat controller in Task 3. The remaining paragraphs in this section will detail the results of the Phase II tasks.

Task 1 – Heliostat Size, Load, and Market Analysis

SubTask 1.1 – Publish Heliostat Size Analysis Results

Subtask 1.1 was to publish the heliostat sizing work developed under this project by UAH. Other heliostat design considerations related to heliostat loads and life were also completed. The summary of UAH-generated publications is:

Publications:

Lovegrove, Keith and Wes Stein, *Concentrating solar power technology - Principles, developments and applications.* 2012. Woodhead Publishing Series in Energy No. 21:

Chapter 17 *Heliostat Size Optimization for Central Receiver Power Plants* presents size analysis based on openly available cost data (Sandia).

ISES Journal, Solar Energy:

Parametric Determination of Heliostat Minimum Cost Per Unit Area

Accepted for publication by the ISES Journal, Solar Energy:

Heliostat Design Considerations - Site Wind Loads Effects on Projected Fatigue Life and Safety Factor

In review by the ISES Journal, Solar Energy:

Wind Gust Distribution Analysis and Potential Effects on Heliostat Service Life, with Allen H. Weber and Steven R. Chiswell, Savannah River National Laboratory

In preparation:

Potential Effect of Dynamic Coupling on Heliostat Failure due to Excessive Load

SubTask 1.2 – Refined Analysis for Wind-Induced Cumulative Fatigue Damage

Subtask 1.2 was to continue the initial fatigue related work started in Phase I. UAH had the complete responsibility for this task. One factor in the sizing related work, was the relationship between heliostat size and natural frequency. In general, having a natural frequency that can be excited by wind-induced loads is not desirable. Figure 1 shows the results of natural frequency calculations. The natural frequency of smaller heliostats is higher, and thus less coupling occurs with wind gusts and vortex shedding occurs at lower loads, both effects increase life for smaller heliostats relative to larger heliostats.

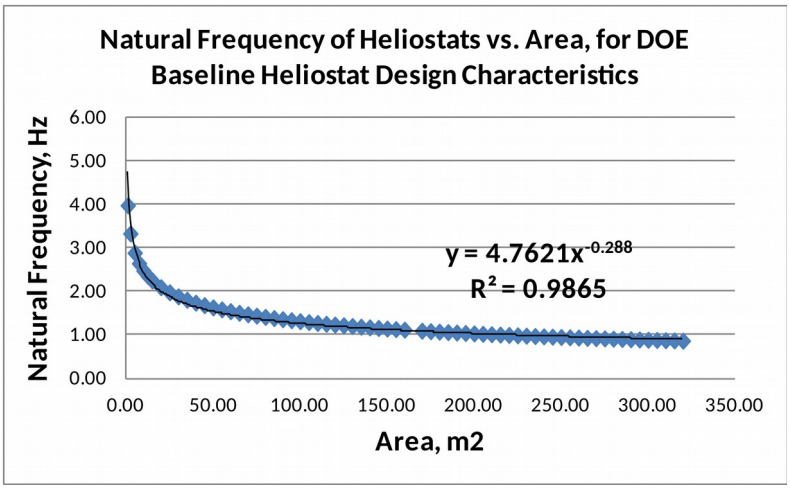

Figure 1 – Natural Frequency Estimate as a Function of Area for a Typical Heliostat

UAH's analysis has led them to conclude that wind load dynamic coupling is far more severe than previously realized over the last 35 years of heliostat development. This has been documented in the previous reports. The summary of this effort is below.

- Parametric analysis shows that fatigue damage is critical.
- Azimuth drive unit emphasized:
  - Typically one of the most costly assemblies in a heliostat
  - Linear actuator elevation drive can be mounted to minimize reversed loads.
  - Number of loads is extremely high. At low wind speeds does not exceed moderate endurance limits and thus should not contribute to fatigue damage.
- Limited data available on loads and relationship to winds (vortex shedding used).
- Realistic endurance limits require high safety factors for a large number of sites.
- Low wind speed sites (10 ft/sec) have far fewer loads above endurance limit than sites with higher wind speeds and thus fatigue is much less of an issue.
- Site with a high average wind speed (e.g., Barstow, CA, 16.3 ft/sec) vs. a site with low average wind speed (10 ft/sec), reduces fatigue life and requires a high safety factor.
- Fatigue life is very strongly dependent on angle of attack (AOA). Sandia 20 degree AOA imposes far higher safety factor than 45 degrees (“feather” heliostats).
- Heliostat designed for moderately high wind speeds (15.8 ft/sec Sandia spec) can have increased area for sites with lower wind speeds and thus reduce $/m2.
- Determined a new design criterion to ensure dynamic loads do not exceed static load safety factor based on fatigue from cyclic wind loads.
- There are many examples of heliostat and dish concentrator failures that may have been due to dynamic load amplification, but, there are no root cause analyses and data on conditions, damage incurred, etc., are sparse.
- This lack of insight poses a risk to developers.
- The approach developed includes determination of the safety factor required to achieve 30-year life, based on wind loads that induce fatigue damage. A sufficiently high safety factor (e.g., 2.0) would satisfy that requirement for representative cases, with a quasi-static load.
- However, the loads are not quasi-static, and have a high degree of load amplification, depending on the damping ratio.
- Recommended approach:
  - Heliostat developer selects a safety factor to achieve 30-year life based on cumulative fatigue damage from vortex shedding and wind gust induced loads, using the method presented in the paper recently accepted for publication.
  - That same safety factor determines the damping ratio needed to ensure that dynamically coupled loads, even under the worst case conditions of angle of attack and wind speed, would not cause failure.
  - For installed fields, fatigue damage effect on life can be estimated. If necessary, heliostats can be stowed at lower wind speeds than legacy specifications require (e.g., 35 mph, fully stowed at >50 mph)

- Vary the stow position orientations to avoid loads being imposed at the same point on internal components

SubTask 1.3 – Market Analysis & Requirements

This subtask was an effort to create realistic heliostat requirements and to engage some large systems integrators to help insure that these requirements are somewhat consistent with a number of central receiver integrators. These companies include Solar Reserve, Abengoa, and BrightSource Energy.

Optical modeling was used to help ascertain some of the heliostat requirements. These include reflector shape, allowable mechanical errors, and tracking requirements. Figure 2 shows the typical Field Input or setup screen from the SolarSim software.

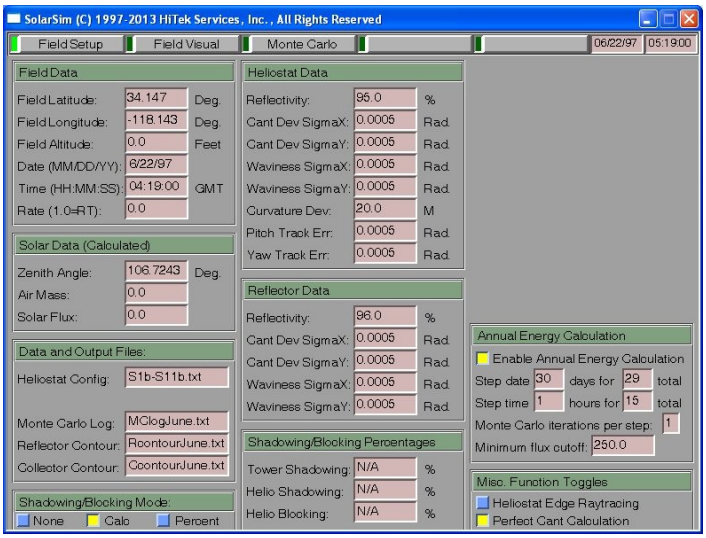

Figure 2 – SolarSim Field Input or Setup Screen

SolarSim allows for various optical errors as a ray moves from the sun to receiver These values include: Cant Deviation (2 planes), Surface Slope Error (2 planes), Curvature Deviation, Tracking Errors (2 planes). For the 100MWe Plant Simulations, all the optical errors were defined as 0.5mr each.

As an example, far-field heliostats were modeled to understand if flat mirrors were sufficient or if curved ones are required. Figure 3 shows a test configuration with a small number of far-field heliostats within SolarSim™. These early results showed that flat mirrors at the farthest distance from the tower spilled over 4% more energy than spherically shaped mirrors.

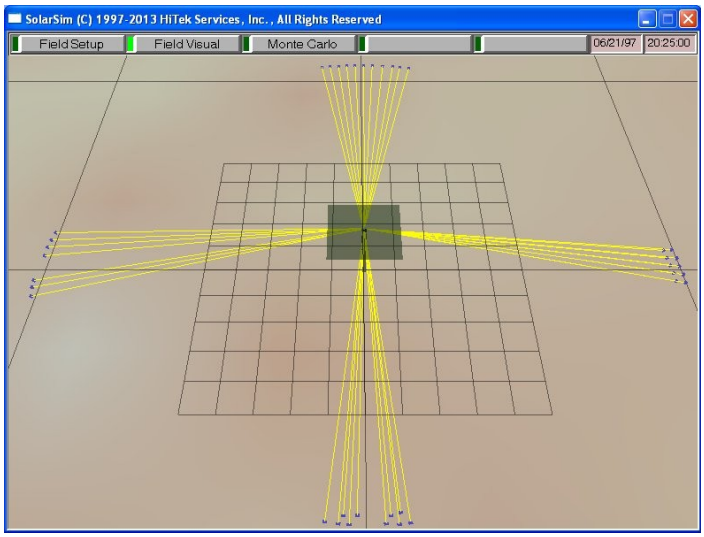

Figure 3 – Overhead View of Far-Field Heliostats in Relationship to the Tower (Center of the Grid)

Further analyses were conducted to try and gather a baseline optical performance for the Solar Reserve Tonopah plant based upon available public information. This was then used to compare the performance of the heliostat under development.

The initial look at annual energy delivered to the receiver of a plant layout that mimics Solar Reserve's Tonopah facility was completed. The first analysis used a $64m^2$ heliostat with 35 flat mirrors ($1.783m^2$) to emulate our best understanding of Solar Reserve's design. This design used 13,100 of these heliostats in the field. The data were computed using our optical modeling software, SolatSim, and then integrating and plotted from a spreadsheet. Figure 4 shows the daily energy intercepted by the receiver shown over more than one year. For purposes of these analyses, the optical efficiency is defined as:

$$\text{Optical Efficiency} = \frac{\text{Energy Hitting the Receiver}}{\text{Total Mirror Area x Sun's Energy per unit area}}$$

For this design, the annual thermal energy to the receiver was about 1.42GW-hr which correlates to a 70% average optical efficiency.

Further analyses replaced the $64m^2$ heliostat with a $10m^2$ version. The field was divided into a number of sectors and the mirror to land ratio in each sector was held consistent between the $64m^2$ analysis and the $10m^2$ analysis. The results from these analyses showed a slightly lower optical efficiency than the baseline design. After further analyses, the optical design using nine (3' x4') flat mirrors was chosen.

The conclusion to this point is that there is little difference in optical efficiency for this design whether four or sixteen mirrors are used for the 10 m^2 heliostat with the modeled receiver. The flux distribution on the receiver is expected to be different as the number of mirrors change if no other factors are considered (e.g., aim point changes, etc.). Another consideration is with that aiming requirements may be less stringent with a generally more compact flux distribution aided by smaller mirrors.

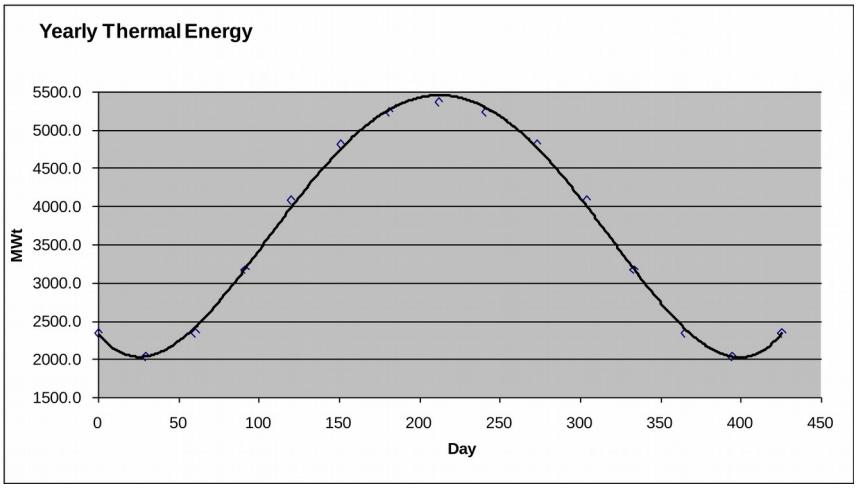

Figure 4 – Daily Energy Intercepted by the Receiver for the 64m^2 Heliostat

DOE provided a number of contacts for central receiver system integrators that could provide their top-level heliostat specification to help ensure our heliostat design is commensurate with what the industry is doing. We received some limited specifications form Abengoa and BrightSource Energy while SolarReserve was unable to provide any information. The initial review of these specifications did not highlight any major disconnect with our performance specifications. Table 1 lists the primary specifications relayed from Abengoa and BrightSource along with the specification HiTek believes is reasonable.

Table 1 – Comparison of Primary Heliostat Specifications from System Integrators and HiTek

	BrightSource	Abengoa	HiTek	Units
Optical Error				
Calm Winds	3	2.82-2.89	3	**mr**
High Winds	4	3.1-4.82	4	**mr**
Max Wind (tracking)	27	35	27	**mph**
Max Wind (stow)	85	90	90	**mph**
Lifetime	25+	30	30	**years**

Task 2 – Drive Unit

This task had three main objectives: (1) to design, fabricate, and test the prototype heliostat drive system, (2) to design and test a novel damping system for a chain drive and (3) to perform accelerated life cycle tests to find weaknesses in the long-term performance of a staged chain drive. Objective #1 was primarily performed by HiTek while the other two objectives were primarily undertaken by UAH. At the end of the project, while many of the azimuth drive components were fabricated, the prototype unit was not completed. UAH developed and tested a number of configurations for the chain damping hardware and developed a novel test apparatus for inducing variable loads into an accelerated-life testing system for the azimuth drive.

SubTask 2.1 – Drive Unit Design and Fabrication

Once the heliostat area was fixed at 10m^2, the azimuth drive design was able to proceed. The final drive design was intended to use the tensioner-damping mechanisms developed by UAH. The version that was under construction when the project ended had tensioner-only mechanisms designed in that were intended to be replaced when the UAH-developed designs were more mature.

This version of the azimuth drive incorporated 5 stages of reduction and a small stepper motor. Further, the control electronics were incorporated into the case top with an integral azimuth encoder. Lastly, the initial design used a centrally located 36" screw jack (see Figure 5) to drive the elevation axis. This was changed near the end of the project to a side mount which cut the jack stroke in half. This change added significant time to the project timeline since it affected multiple components of the heliostat.

Figure 6 shows an exploded view of the azimuth drive. Its features include: an extensive use of COTS components,five stage design: 4 single strand chain, 1 toothed belt, a 24,309 to 1 drive ratio, swing-arm tensioner designs that can be enhanced with damping components as they become available, a case design: optimized for ease of fabrication, that incorporates features that manage internal component deflections and enhance unit operational life, an axle center distance optimized to manage chain deflection, designed for survival of 50 mph gust wind any orientation and 90 mph gust in wind stow. All the components showed positive margins with a 2.0 factor-of-safety.

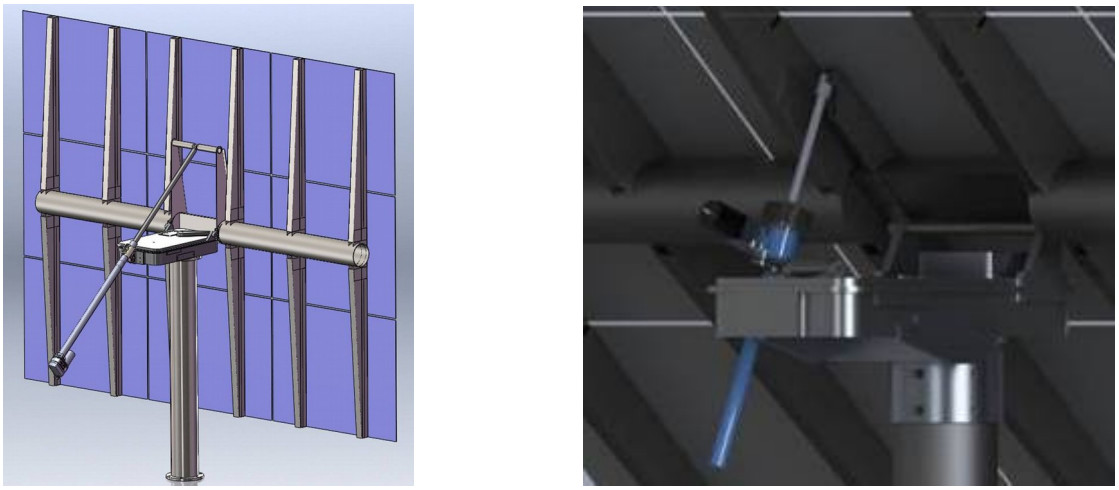

Figure 5 - 1st Concept with 36” Jack (left) and Final Concept with 18" Side Mounted Jack (right)

Additionally, the final design for the controller PCB required some changes to the azimuth case top design. The control electronics (see Figure 7) sits on top of the azimuth drive and all wiring now rotates with the heliostat which reduces wire related fatigue failures from constantly flexing the power and control wires as the drive system articulates.

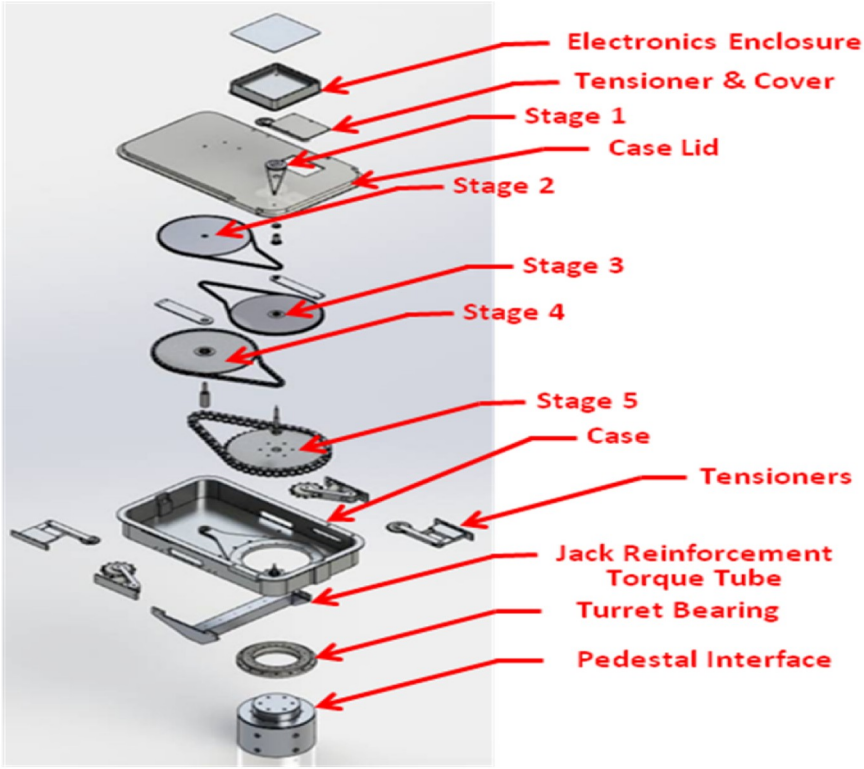

Figure 6 – Exploded View of the Azimuth Drive

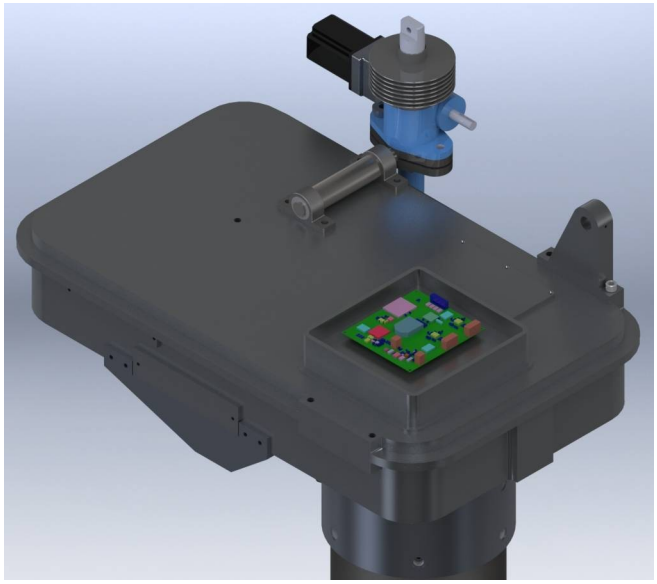

Figure 7 – Location of the Controller PCB atop the Azimuth Drive

Chain Drive Damping Work

In conjunction with the wind load and fatigue analyses, we sought to diminish the effects of these anticipated cyclical loads through the use of a novel damping mechanism. UAH led the effort to design and test a mechanism that acted as a chain tensioner with integral damping. The USISTC 3-stage chain drive used in the Phase I accelerated wear tests was modified for this development to test the different damping mechanisms.

This unit has been equivalently tested to over 100 years of load cycles in Phase 1. Figure 8 show the original single spring tensioner.

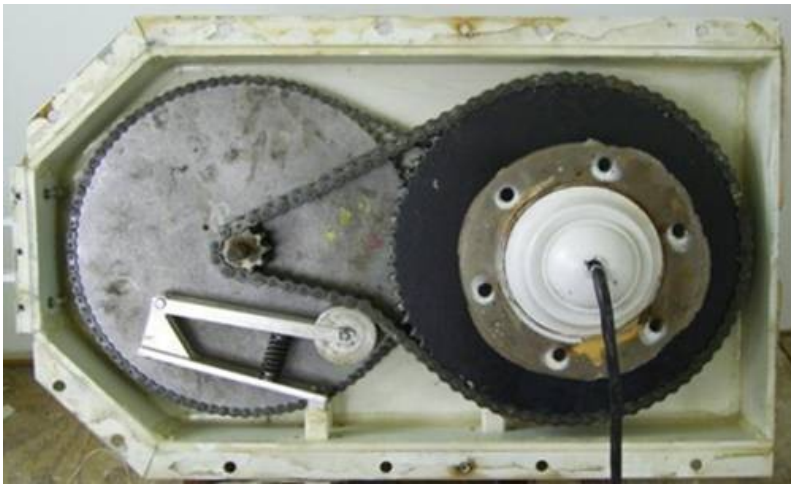

Figure 8 – Interior of USISTC Chain Drive used for Lifecycle Tests

As part of the preliminary tests, the drive compliance was measured to garner baseline performance. Figure 9 shows the angular deflection versus load torque for a few tensioner settings. As can be seen, there is significant deflection with load for this original drive design.

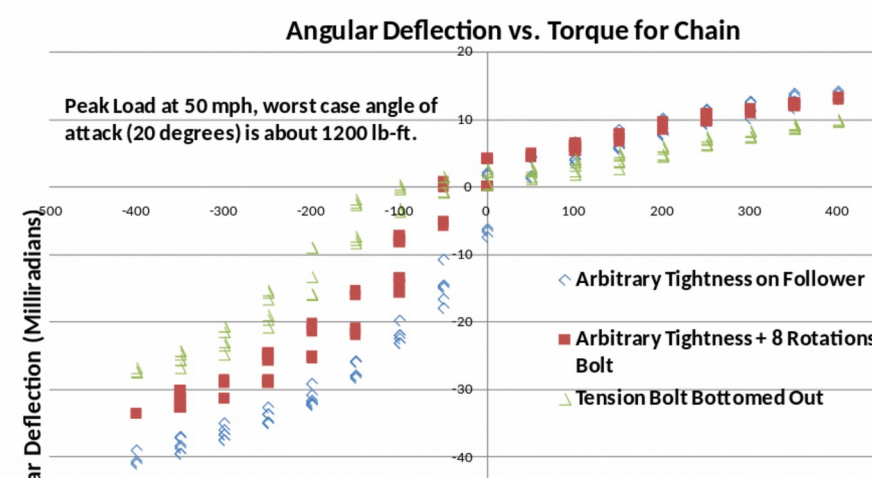

Figure 9 - Angular Deflection of Drive Unit and Pedestal-USISTF Prototype Azimuth Drive Unit for 9.2 m^2 Heliostat

Figure 10 shows the assembled drive unit with the modified tensioner-damper. Once the initial tensioner-damper mechanism was installed, it was tested to understand its effect on the drive's dynamic response. This response comparison (original tensioner-only vesus tensioner-damper) is shown in Figure 11. The data showed that the damping of the original drive mechanism is "low" and the addition of the Sorbothane-based damper increased the damping coefficient. However, these initial tests also showed that we must more fully enclose the damper mechanism to prevent extruding the Sorbothane material during operation.

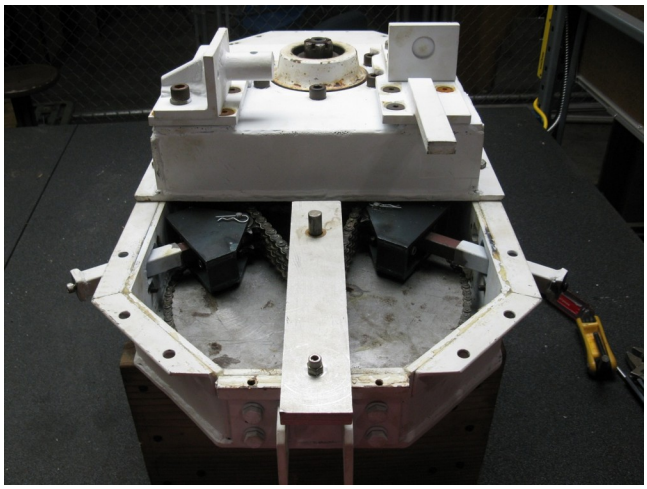

Figure 10 – Modified Staged Chain Drive with Tensioner-Dampers Installed

In an effort to reduce the deflection under load, an improved tensioner design was conceived and tested. The angular deflection vs. torque results are displayed in Figure 12. As can be seen, the improved tensioner design significantly reduced the angular deflection as compared to the original design.

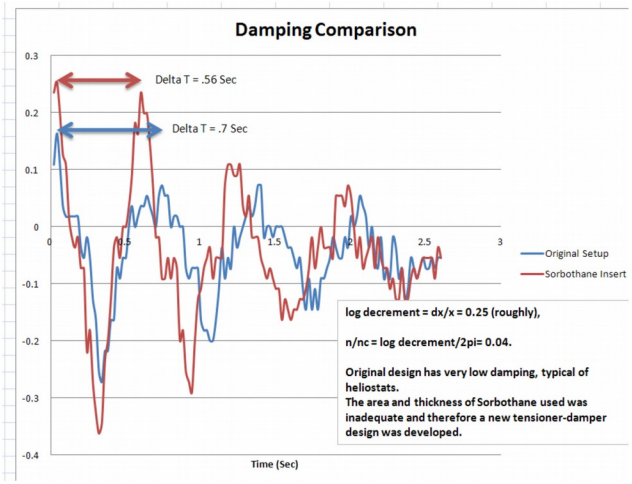

Figure 11 – Initial Response Data Comparing the Stock Drive with the 1st Dampener Concept

To understand the pedestal's contribution to the angular deflection, a series of tests were conducted with the results shown in Figure 13. These results indicate that the pedestal's contribution to the overall deflection in the preceding measurements is not insignificant. A small effort was expended to develop a novel method for stiffening the pedestal for rotational loads. The method will be evaluated at some point in the future to determine its overall cost and performance impact on the heliostat. The last series of deflection test results are shown in Figure 14 and marked improvement over the original drive stiffness.

When the project ended, UAH had demonstrated theses drive characteristics:

- Zero backlash, zero shaft endplay, new tensioner has 5X stiffness.
- Concrete-stiffened pedestal with 4X stiffness of steel pipe.

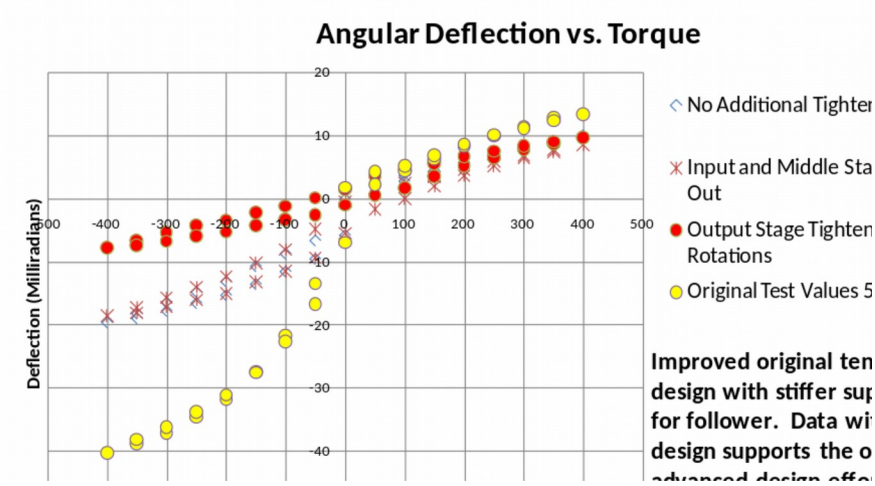

Figure 12 - Angular Deflection of the Modified USISTC Drive Unit and Pedestal

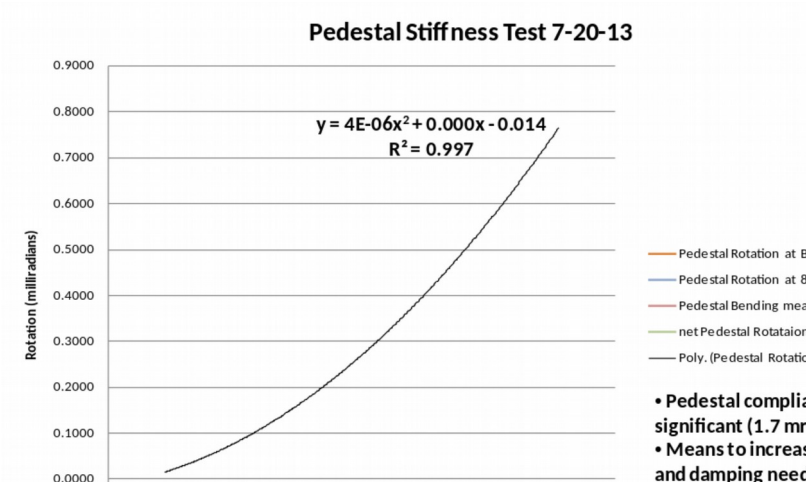

Figure 13 - Angular Deflection of the USISTC Pedestal

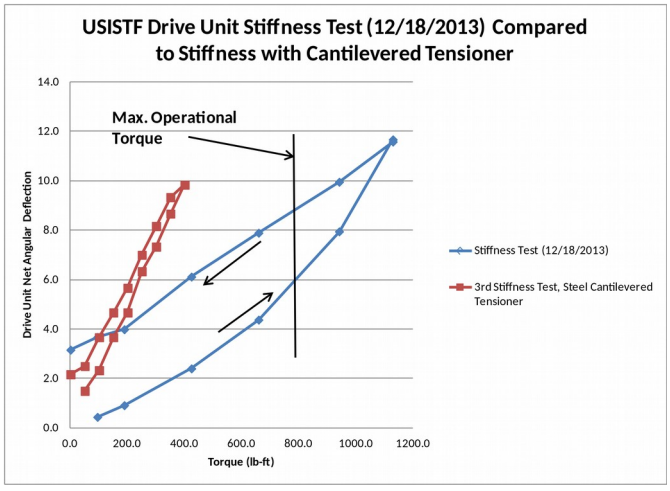

Figure 14 – Comparison of the Azimuth Drive Deflections Between the Original Tensioner and the Updated Tensioner/Damper Hardware

- Developed a new design criterion:
    - To have the same safety factor, S, for quasi-static wind load induced fatigue failure over 30-years, the dynamic load must not exceed that maximum static load. Damping is the only intrinsic way to avoid this and the design condition is:
        - Damping ratio, n/nc = 1/2S. For S = 2, the damping ratio must be at least 0.25, well above typical values of 0.05 to 0.1. Otherwise, dynamic loads can be several times maximum static load.
- New tensioner-damper increases stiffness by a factor of five over initial cantilevered design. Stiffness now limited primarily by chain.
- The conclusions from this UAH-derived work are (1) that pedestal rotational deflections may not be insignificant and should be analyzed to understand their contribution to beam movement with wind loading, (2) a single mechanism that combines the chain tensioning function with a damping mechanism is desirable and (3) tests with the Sorbothane-based mechanism are promising but require further work to increase effectiveness and reduce hysteresis.

SubTask 2.2 – Accelerated Life Testing

UAH designed, fabricated, and tested a unique test bed for subjecting an azimuth drive to dynamic loads simulating wind and control loads. Figs. 15 and 16 depicts the test rig.

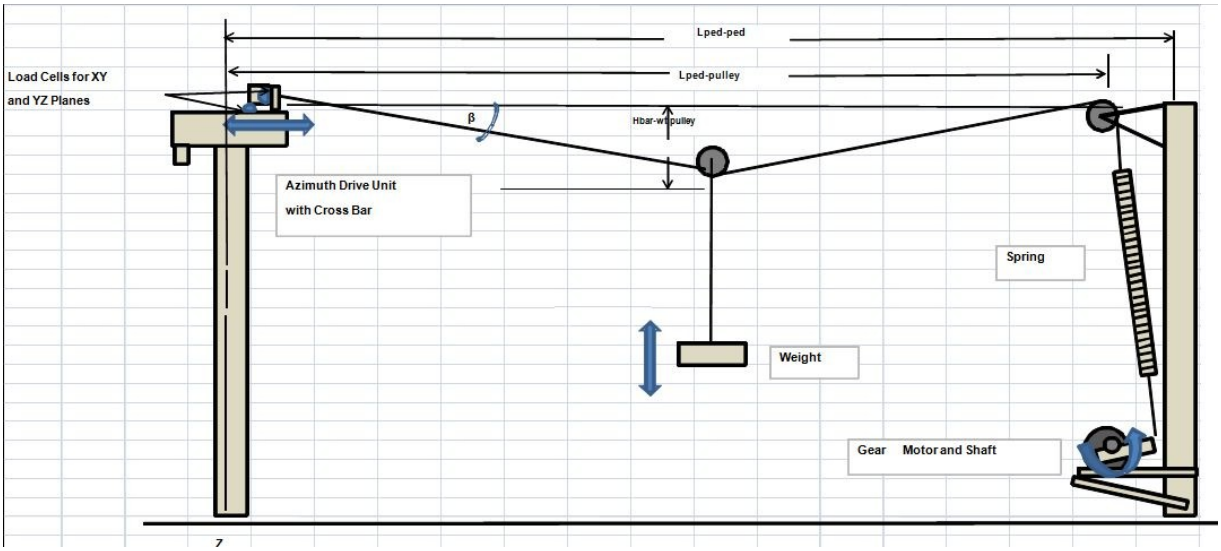

Figure 15 – Depiction of Test Rig to Simulate Dynamic Loads Induced by Wind and Control Inputs

This test bed design is intended to simulate both relatively slowly varying wind gust loads and relatively rapid vortex shedding loads. Motor pulses are used, rather than simply moving heliostat back and forth, to simulate these impulse loads on the input stage. A central weight moves up and down with sinusoidal variation in torque that simulates wind gusts. A motor-spring arrangement superimposes a more rapidly varying

simulated vortex shedding load into the drive system. The modified chain drive for the 9.2 m^2 USISTF heliostat was used for these tests.

To understand what a typical vortex shedding frequency may be for our heliostat, we computed the Strouhal number. For typical flat plate flows, the Strouhal number is approximated as a constant value of about 0.2. The vortex shedding frequency can then be approximated by equation St = fL/V where St = Strouhal Number = constant = 0.2, f = frequency, L = characteristic length, V = fluid velocity. For a nominal 10m^2 heliostat in "high" winds, L = 10 feet and V = 50 feet per second (34 mph). The computed vortex shedding frequency is 1Hz. This is the frequency used as the RPM in the "Vortex Shedding Drive Motor" in the oscillating load test rig. UAH ran about 30,000 additional cycles simulating vortex shedding loads, plus, tests for compliance. The input shaft broke in fatigue, somewhere around 150 years of equivalent life, and after very high peak moment loads had been imposed (about 90% of the maximum wind load of about 1200 ft-lbs).

Figure 16 – Rig to Simulate Dynamic Loads (l) with close-up of vortex impulse load generator (r)

Task 3 – Heliostat Control

The primary objective of this task was twofold: (1) design, fabricate, and test the baseline autonomous heliostat controller for near-term use and (2) to prototype various elements of an advanced autonomous heliostat controller that seeks to reduce the controller costs by eliminating as many electronic components as possible. When this phase of the project was proposed, UAH was going to undertake the advanced control work and provide a majority of the labor to accomplish the task at no-cost to the project. By the time the phase was started, UAH's conditions had changed and they could no longer provide that assistance to the project. This part of the task was delayed for some time as UAH sought ways to complete the work under the original funding level.

SubTask 3.1 – Baseline Autonomous Heliostat Controller

The baseline autonomous controller is the next-generation built from our experience with the Phase I demonstrator control hardware. The impetuous has been to reduce the Category 3 costs to keep driving the overall heliostat \$/m^2 down. The changes include:

- Increasing encoder resolution while decreasing cost

- Reducing drive motor cost
- Balancing electronics parts count with firmware development time & cost
- Increase use of power-saving methods to minimize battery size and cost

The final architecture included two just two printed circuit board assemblies: the main control board and the elevation encoder.

The development included fabricating test PCBs that were incrementally populated to test the various control subsystems.

The final PCB for the baseline controller underwent testing as the various sections of the PCB incrementally populated. These sections included the PV array charge controller, the DC-DC converter, the wireless interface, the motor controllers, the encoders, and the processors. This version of the controller also contains a SD card interface to store data during the various testing phases. The SD card in not anticipated to be used in an actual production version.

Once the controller had successfully completed its electrical functional tests, it was mounted to an existing azimuth chain drive to enable further simulated tracking tests while the actual azimuth drive was undergoing fabrication. Figure 17 shows the bare controller PCB installed on the test drive with an elevation jack (bottom of figure) to enable the simulation of both drive axes.

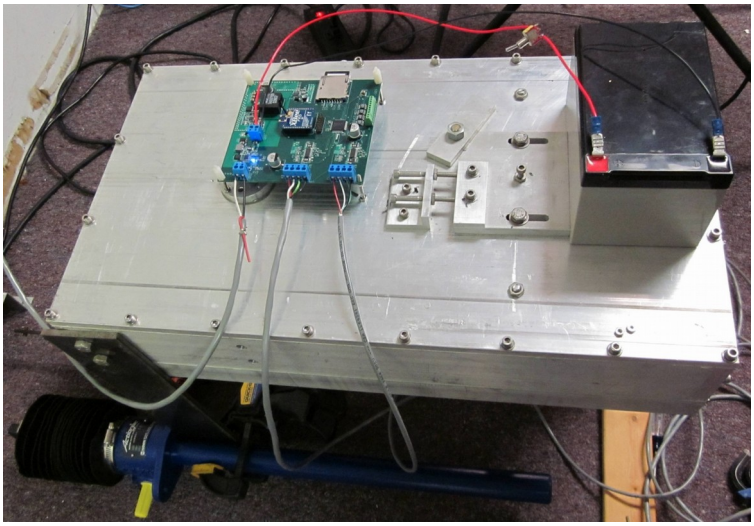

Figure 17 – Controller Undergoing Tests While Driving a Previous Azimuth Drive

When the project ended, the baseline controller was ready to be integrated into the heliostat system and undergo further functional tests.

SubTask 3.2 – Advanced Heliostat Controller

As discussed above, this task was undertaken by UAH. The prototype subsystem brass board was assembled (stepper motors, control software for tracking). The addition of a wireless master control system and a PV/battery charge controller were in progress

when the project ended. A new UAH-funded initiative has allowed work to continue on this task through the end of the spring 2014 semester.

Task 4 – Heliostat Integration

The primary objective of this task was twofold: (1) design and fabricate the balance of heliostat components not covered in Tasks 2 and 3 and (2) to integrate and perform functional tests for the assembled heliostat. The balance of heliostat parts included the mirrors, mirror support structure, and pedestal. After discussions with DOE personnel, it was determined that conventional 2nd surface glass mirrors were the safe design choice. After the mirror technology was determined, the size, number, and placement were taken from the optical analyses conducted under Task 1. The mirror support structure went through various iterations to find a low-weight version that presumably would also be low-cost in mass production (assuming no exotic processes in its fabrication). The pedestal was a conventional steel tube intended to be driven into the ground like a wood fencepost.

A series of analyses were undertaken to develop a family of design curves where the mirror thickness and spacing of a simple support structure were varied. During the analyses, it became apparent that few low-cost solutions exist once the glass mirror thickness is fixed at 4mm.

Figure 18 shows a rendering of the final version of the prototype heliostat. This view highlights the side-mounted elevation jack and the PV array (right side of figure) used to power the heliostat.

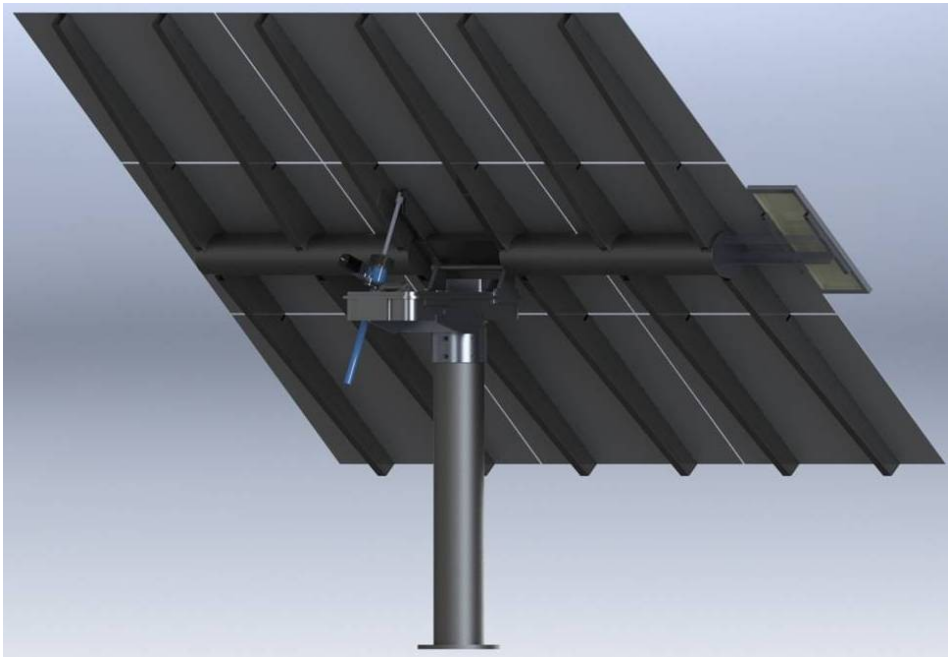

Figure 18 – Rendering of the Rear View of the Prototype Heliostat

The features of the mirror support structure include:

- All Steel Structure
  - Center Torque Tube
  - Welded Flanges to mount Ribs
- Ribs

  - 2 per Reflector
  - Tapered from 6” deep at torque tube to 3” at end
- Reflectors bonded to one face of rib
- Drive Interface separates jack load path from mirror support structure

Two deflection analyses were conducted to verify the design at two load conditions: (1) gravity bending while flat on its back and with a 12 meter per second wind load with a 30 degree elevation angle. For each case, two methods to determine the peak deflection were used: (1) handbook methods and (2) Finite Element Analysis. The maximum deflection was experienced in corner of heliostat and the deflections from two methods were within 2% of each other. The FEA determined peak deflection was 0.02537” and the hand analysis deflection was calculated at 0.02487”.

For the FEA, we modeled half of structure (making use of symmetry), constrained the reactions at torque tube center, and applied mass equivalent loads to the ribs and end of torque tube. The results (see Figure 19) showed the maximum deflection occurs at end of rib furthest from center (as expected) and that the deflected shape has a convex character.

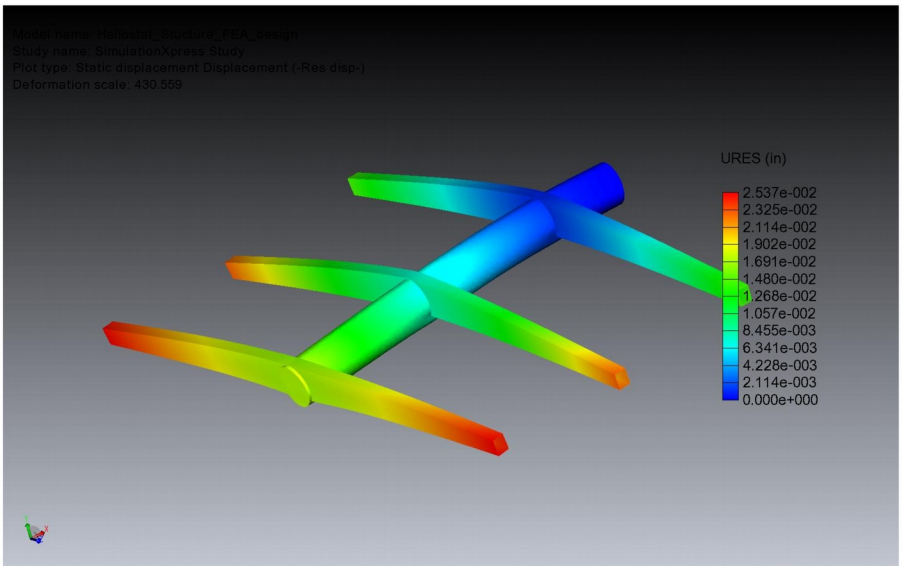

Figure 19 – Finite Element Analysis Deflection Results

The angular deflection analysis was done using handbook methods similar to deflection analysis. The results showed that the worst angular deflection occurs at the greatest deflection points (end of furthest beam) and 0.32 mrad for the wind load case and 0.74 mrad for the gravity bending case.

The fixture required to accurately bond the mirrors to the mirror support structure is shown in Figure 20. This fixture design is based upon previous HiTek-developed mirror bonding techniques and allows all nine mirrors to be bonded in one operation. The tool is adjustable and allows for various canting schemes. The mirrors were to be canted to focus on-axis at the heliostat-to-target distance for the initial tracking tests.

This fixture has two functions. The first is to use it as a fixture to align the various parts of the mirror support structure (torque tube to rib alignment) and then it is used to accurately bond the mirrors to the completed mirror support structure.

When the project ended, the mirror bonding fixture was ready to use, the pedestal and torque tube were ready for welding, and the balance of the mirror support structure was on order (subsequently cancelled).

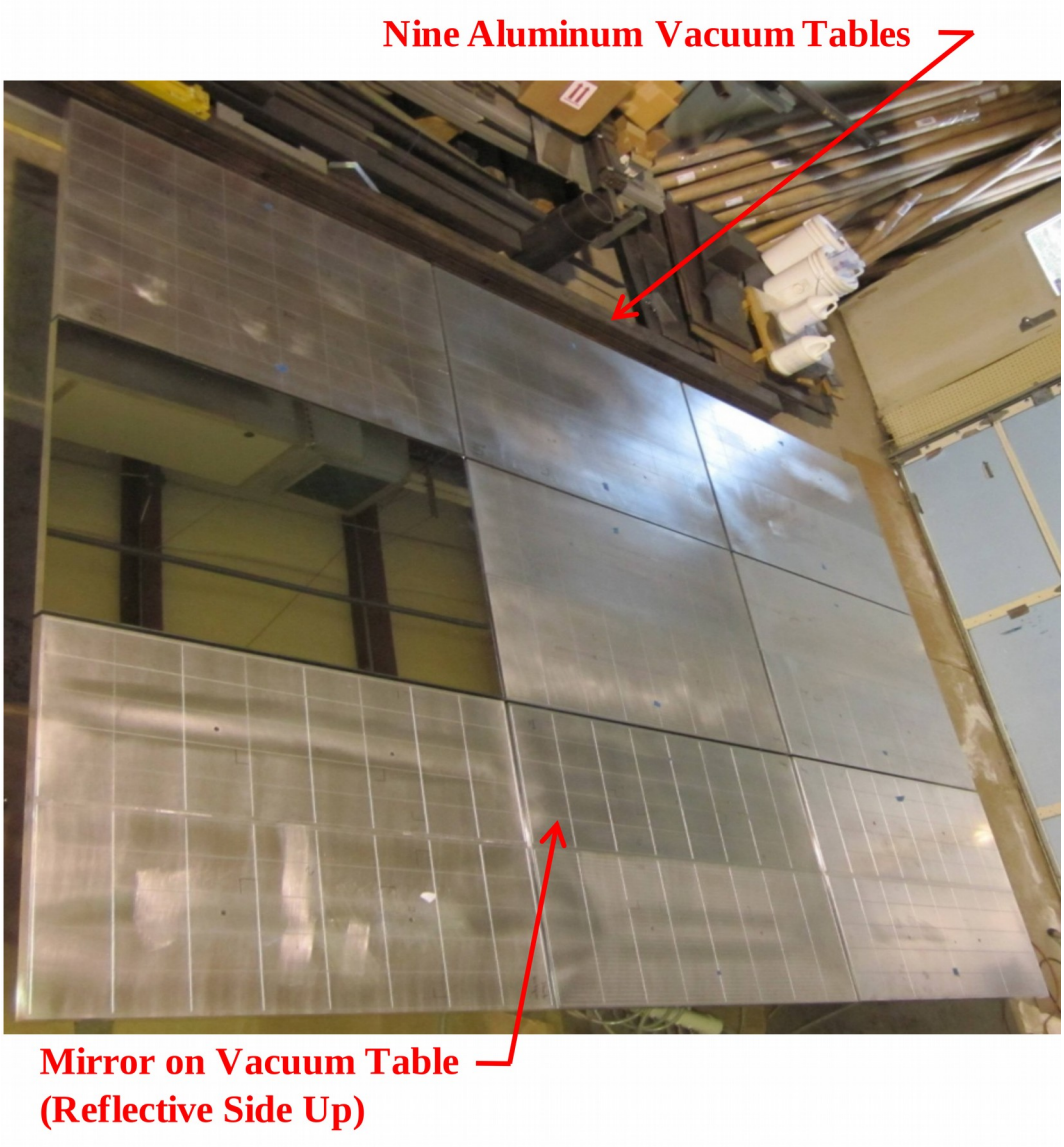

Figure 20 – Mirror Bonding Fixture

Task 5 – Prototype Heliostat Testing

The primary object of this task was to expand upon the basic functional and reflected beam tests that would be done under Task 4. As such, on-sun tests were to be conducted for beam quality over a substantial period of time and under varying conditions. The test results were to then be compared with the analytical results from detailed ray-tracing analysis and further used to measure the unit's tracking accuracy.

Our test plans included:

- All tests will be conducted at HiTek
- Using an updated DIR/BCS system for reflective surface evaluation and tracking accuracy determination
- Gathering time-stamped reflected beam images and then process this image information (not in real-time) to compute the tracking accuracy in both axes.
- The captured image data will then be used to verify the beam quality by comparing a subset of the images with iso-flux contour maps developed from SolarSim analyses.

Figure 21 shows the heliostat and target locations. The test hardware and software was designed to gather this simulated east-field heliostat with large off-axis errors at the start of the day and much more on-axis performance in the late afternoon.

Figure 21 – Satellite View of HiTek's Facility with Heliostat and Target Locations

To determine the size of the Beam Characterization Systsem (BCS) target, SolarSim was used to calculate the reflected beam iso-flux contours for the heliostat throughout a typical day. The nine flat-mirror heliostat model was analyzed and the results are displayed in Figure 22. From this data, we determined that a 16' x 16' target would be large enough to capture the reflected beam. The target surface is a fabric outdoor movie screen supported by a steel frame that can be moved to preset locations, as needed.

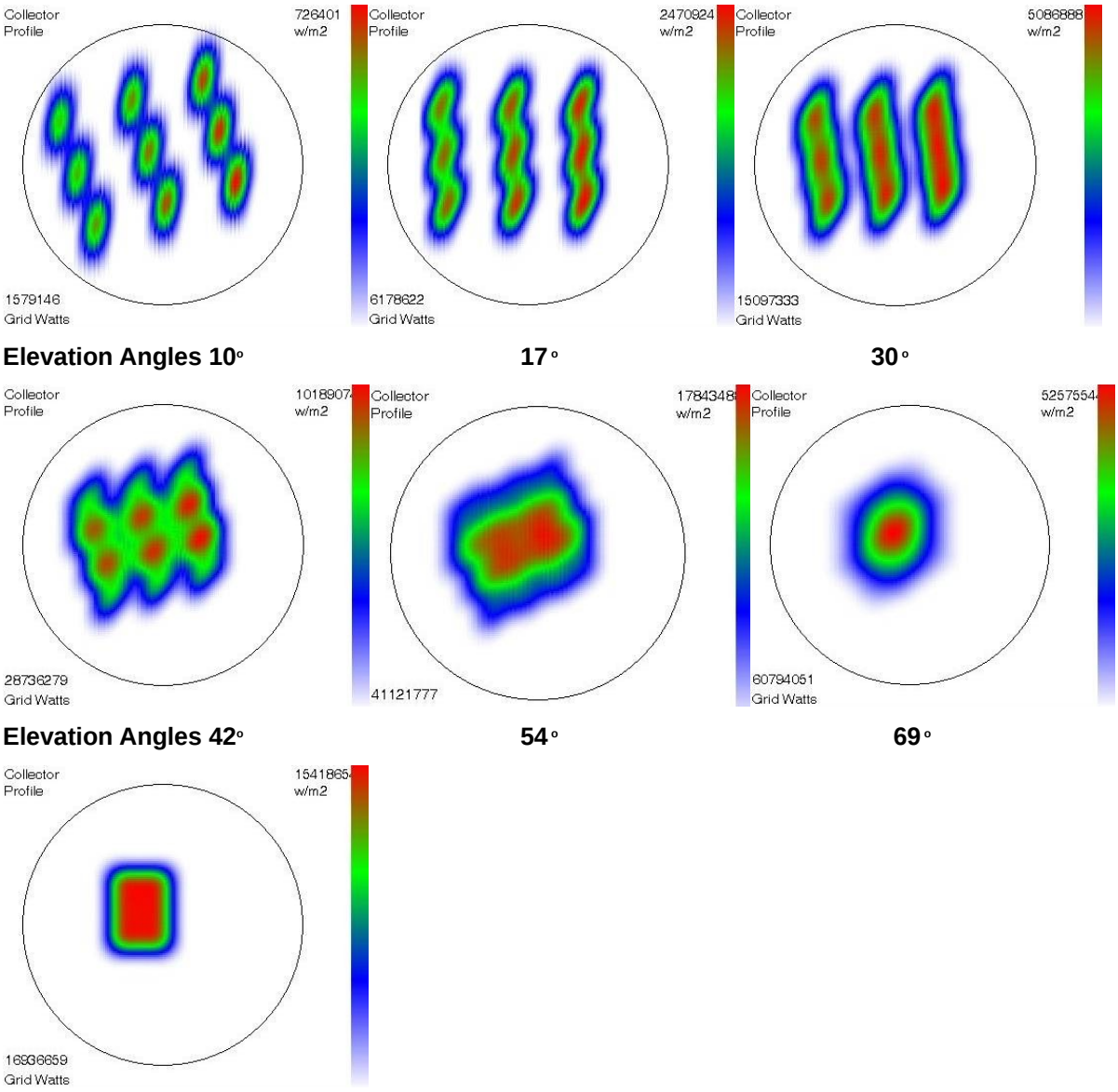

Figure 22 – Iso-flux Contours Predicted from SolarSim Ray-Tracing Analysis for the Prototype Heliostat with Nine Flat Mirrors Canted On-Axis at the Heliostat-to-Target Distance.

The BCS camera, lens, and acquisition software were tested for image size and clarity. The test images were deemed satisfactory for subsequent post-processing. However, the need for a better aiming system was noted and addressed with the addition of a more rigid camera manual tilt/pan/roll mount. When the project ended, the BCS system software and hardware was ready for initial on-sun testing.

Plans for Next Quarter: This is the final report. There are no further activities.

References: None